Multiscale structure of magnetic fields in the heliosheath

L. F. Burlaga,[1] N. F. Ness,[2] and M. H. Acũna[3]

Received 12 May 2006; revised 16 June 2006; accepted 23 June 2006; published 22 September 2006.

[1] Voyager 1 (V1) crossed the termination shock, leaving the solar wind and entering the heliosheath. This paper analyzes the magnetic field observed in the heliosheath from day of year 1 to 308, 2005. The average of the magnetic field strength B is 0.104 nT, but it is highly variable, and its profile appears filamentary. Some sectors and sector boundaries were observed. The daily and hourly averages of B in the inner heliosheath have Gaussian distributions. The widths of the daily and hourly distributions of B are the same within the uncertainties, consistent with a scale invariance of the distribution of B. The distributions of daily and hourly averages of the azimuthal and elevation angles in the heliosheath resemble those in the solar wind. The magnetic field strength in the inner heliosheath has a multifractal structure on scales from ~2 to 16 days. The multifractal structure can be described by a binomial multiplicative cascade model. The multifractal spectrum of the magnetic field fluctuations in the heliosheath is narrower than that in the distant solar wind. The intermittency exponent decreases by a factor of 3.4 from 0.072 in the distant solar wind to 0.021 in the heliosheath. We also analyzed the multiscale structure of B(t) using wavelets. On an intermediate scale, the magnetic field of the heliosheath contains a quasiperiodic variation suggesting that the effect of solar rotation was observed in the heliosheath beyond 95 AU.

Citation: Burlaga, L. F., N. F. Ness, and M. H. Acũna (2006), Multiscale structure of magnetic fields in the heliosheath, *J. Geophys. Res.*, *111*, A09112, doi:10.1029/2006JA011850.

1. Introduction

[2] This paper analyzes the multiscale structure of the magnetic field strength in heliosheath on scales $\geq$1 day, as observed by Voyager 1 from DOY (day of year, 1 January = 1) 1 to 308, 2005. The heliosheath is a region extending from the termination shock to the heliopause and eventually interstellar medium [*Axford*, 1972; *Parker*, 1963; *Hundhausen*, 1972]. Voyager 1 (V1) crossed the termination shock on 16 ± 1 December 2004, the uncertainty being due to a data gap [*Stone et al.*, 2005; *Gurnett and Kurth*, 2005; *Decker et al.*, 2005; *Burlaga et al.*, 2005], and it has been located in the heliosheath since that time. Owing to gaps in the data coverage by the Deep Space Network, data are available for only 8–12 hours each day, typically. Magnetic field observations have been made by the magnetic field experiment on V1 [*Behannon et al.*, 1977] from launch in 1977 to present.

[3] The distributions of hourly and daily magnetic field strengths B in the heliosheath were found to be Gaussian from the interval DOY 1 to 110, 2005 [*Burlaga et al.*, 2005] and from DOY 1 to 125, 2005 [*Burlaga et al.*, 2006a]. In this paper we analyze a larger data set, from DOY 1–308, 2005, where a filamentary structure in the magnetic field strength profile seems to be present. Section 2 shows that for this 308 day interval the distributions of B are Gaussian. The distributions of the azimuthal and elevation angles in the inner heliosheath are similar to those observed in the distant supersonic solar wind.

[4] Changes in the magnetic field strength in the heliosheath on scales from 1 to 16 days have a Tsallis probability distribution function [*Burlaga et al.*, 2006b]. The Tsallis distribution, derived from an entropy principle, describes a system with a hierarchical structure in phase space, such as occurs when there is a nonlinear cascade of energy or magnetic flux across a range of scales. *Leubner and Vörös* [2005] introduced a bi-kappa function to describe turbulence at small scales in the solar wind, but the complexity of this function is not needed to describe the magnetic field. A relation between the Tsallis distribution and the multifractal spectrum in turbulence was suggested by *Arimitsu and Arimitsu* [2000, 2002]. Thus one might expect to observe a multifractal structure in the heliosheath on scales of days. Section 3 demonstrates that a multifractal structure is present in the magnetic field of the inner heliosheath, and it discusses the properties of this structure. The multifractal formalism describes the nonlinearity, intermittency, and scaling symmetry of the magnetic field fluctuations quantitatively, and it provides functions that can be compared directly with data.

[5] The multiscale structure of the heliosheath magnetic field on scales $\geq$1 day is analyzed using wavelets in section 4. Intermittent, bursty signals were observed at the smallest

[1]Laboratory for Solar and Space Physics, NASA Goddard Space Flight Center, Greenbelt, Maryland, USA.
[2]Institute for Astrophysics and Computational Sciences, Catholic University of America, Washington, D. C., USA.
[3]Planetary Magnetospheres Laboratory, NASA Goddard Space Flight Center, Greenbelt, Maryland, USA.

0148-0227/06/2006JA011850

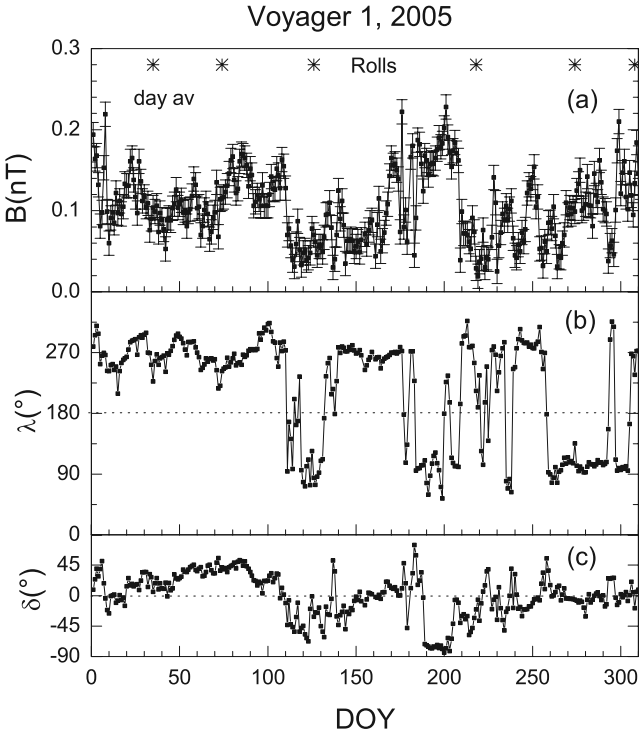

Figure 1. Daily averages of (a) the magnetic field strength, (b) azimuthal angle λ, and (c) elevation angle δ.

scales, and a quasiperiodic component with a period near the solar rotation period was observed at intermediate scales. Section 5 gives examples of the kinds of structures that produce the multifractal spectra, Tsallis distribution functions, filamentary structure, and jumps in the heliosheath magnetic field strength.

2. Large-Scale Structure

2.1. Observations of B(t)

[6] Daily averages of the magnetic field strength B from DOY 1 to 308, 2005 are shown in Figure 1a. This interval represents the "fully processed" data containing all of the calibrations and corrections that are required to derive the highest quality data that were available at the time this paper was written. The representative error bars on B are ≈±0.015 nT, the estimated 1 σ error due to both systematic and random effects. Even after corrections are made, residual systematic errors remain in the measurements (e.g., depending on how the spacecraft magnetic field varies between the rolls at ≈3 month intervals and on errors introduced by the telemetry system); it is not possible in general to estimate these uncertainties more accurately. The average magnetic field strength in this 308 day interval is $\langle B \rangle = 0.104 \pm 0.002$ nT, where the uncertainty here is the standard error in the mean. The standard deviation is SD = 0.043 nT, and the minimum and maximum values of B are 0.02 nT and 0.23 nT, respectively. The profile of B(t) shows large jumps in B and gives the appearance of an underlying "filamentary" or multiple flux tube structure, with the largest "filaments" having scales of the order 50 days.

[7] Daily averages of the azimuthal angle λ and elevation angle δ from DOY 1 to 308, 2005 are shown in Figures 1b and 1c, respectively. Error bars for the angles are not shown since they depend on many factors. The uncertainties in the angles are large (of the order of ±90° for λ and ±45° for δ when B is weak, <0.05 nT) and even larger when the δ is large (which is difficult to determine because of the uncertainties in δ). Thus the profiles for λ(t) and δ(t) in Figure 1 are less quantitative and more qualitative. A "sector structure" seems to be present in λ, because there are intervals where λ fluctuates about ≈270° and ≈90°, and because there are some abrupt transitions between these two states. Most of the sectors and sector boundaries are not well defined, and there is no recurrent or even quasi-recurrent sector pattern. Nevertheless some sectors and sector boundaries are present in the interval considered. Data gaps, as noted earlier, enhance this appearance.

2.2. Distributions of the Magnetic Field Strength

[8] The distribution of the daily averages of B in Figure 1a is shown in Figure 2a. Each of the points is the number of days (number of days $\equiv N_i$) with B in bin i, and the error bars are $\pm\sqrt{(N_i)}$. The dashed curves are the 95% confidence intervals. The solid curve in Figure 2a is a fit of the daily average observations to the Gaussian distribution $B = B_o + A \times \exp(-2 \times ((B - B_c)/w)^2)$ where the parameters are $B_o = -1.0 \pm 6.5$ (consistent with no offset of the Gaussian distribution), $B_c = 0.100 \pm 0.004$ nT, $w = 0.096 \pm 0.016$ nT, and $A = 54 \pm 6.7$. The coefficient of

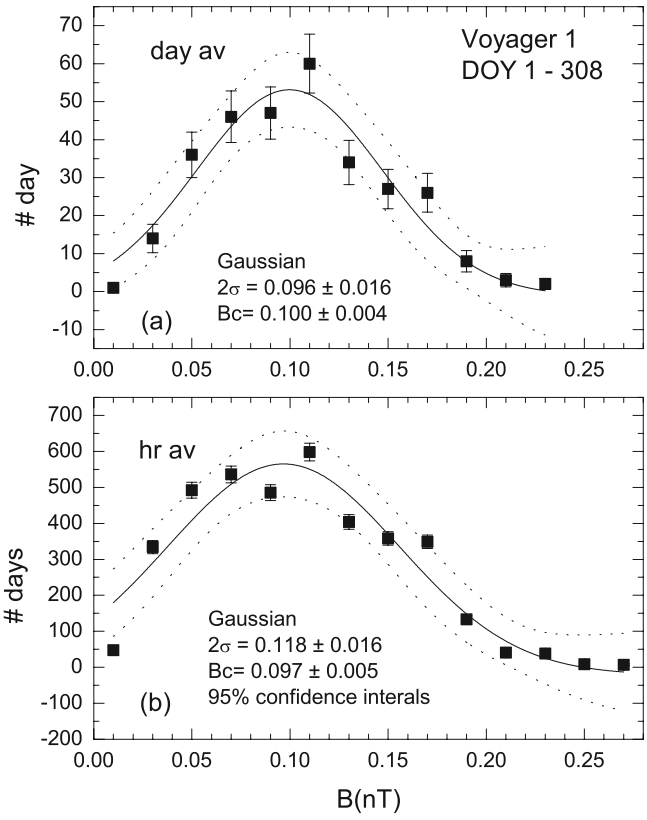

Figure 2. (a) Distribution of daily averages of the magnetic field strength (points) and a Gaussian fit to the data (solid curve). (b) Distribution of hourly averages of the magnetic field strength (points) and a Gaussian fit to the data (solid curve).

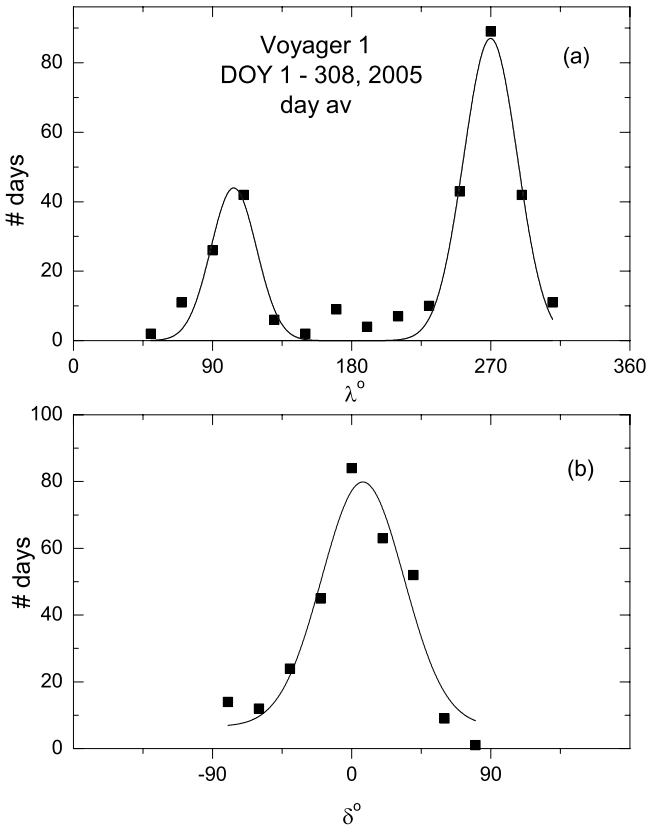

Figure 3. (a) Distribution of daily averages of the azimuthal angle. (b) Distribution of daily averages of the elevation angle.

determination is $R^2 = 0.92$. Thus the distribution of daily averages of B in the heliosheath from DOY 1–308 is Gaussian within the uncertainties, as *Burlaga et al.* [2005, 2006a] found for shorter intervals of time. The Gaussian distribution is in contrast to the nearly lognormal distributions found in the solar wind [*Burlaga*, 1995, 2001]. It is also significant that the $B(t_i)$ observations have a Gaussian distribution even though the profile seems to be filamentary with some large jumps and peaks in B.

[9] The distribution of the hourly averages of B from DOY 1–308, 2005 is shown in Figure 2b. The distribution, error bars and 95% confidence intervals were computed in the same manner as those for the daily averages of B in Figure 2a. One might fit the observations with a skewed distribution rising steeply from B = 0, but the observations are within the 95% confidence intervals for a Gaussian distribution. In particular, fitting the observations to the Gaussian function $B = B_o + A \times \exp(-2 \times ((B - B_c)/w)^2)$ gives the parameters are $B_o = -21 \pm 56$ nT ≈ 0 nT, $B_c = 0.09 \pm 0.005$ nT, $w = 2\,\sigma = (0.118 \pm 0.016)$ nT, $A = 586 \pm 60$, and the coefficient of determination is $R^2 = 0.92$. Thus the distribution of hourly averages of B in the heliosheath from DOY 1–308 is also Gaussian within the uncertainties. The width of the distribution of hourly averages of B (w = 2 × the standard deviation = 0.849, the width of the peak at half height) is $w = (0.059 \pm 0.008)$ nT, which is comparable to the width of the distribution of daily averages of B, $w = (0.048 \pm 0.008)$ nT. The results are consistent with a scale invariance of the distribution of B on scales from 1 hour to 1 day, within the uncertainties.

2.3. Distributions of Daily Averages of Magnetic Field Directions

[10] The distribution of daily averages of λ and δ from DOY 1–308, 2005, are shown by the points in Figures 3a and 3b, respectively. Two Gaussian distributions of the form Equation: $\lambda = \lambda o + (A/(w \times \sqrt{(\pi/2)})) \times \exp(-2 \times ((\lambda - \lambda_c)/w)^2)$ provide a good fit to the observations, with a coefficient of determination $R^2 = 0.96$. The excess of points near λ = 180° is a consequence of taking daily averages of points that fluctuate about the values λ = 0° and 360°, which represent the same direction.

[11] The peak values of the two Gaussian fits occur at $\lambda_{c1} = 104° \pm 2°$ and $\lambda_{c2} = 270° \pm 1°$. The uncertainties are only the statistical errors derived from the fits; the additional uncertainties related to systematic effects are significantly larger, but they cannot be determined precisely. The values of λ_c are close to the Parker spiral values for large distances from the Sun, $\lambda \approx 90°$ and 270°. This agreement with the nominal spiral angles is partly a consequence of the assumption made in processing and calibrating the data, namely, the average of the radial component of the magnetic field $\langle BR \rangle = 0$ for an interval of 52 days centered on each of the S/C rolls, whose times are indicated by the asterisks at the top of Figure 1a. This assumption is made because the spacecraft rolls only about one axis, very close to the **R** direction, so that the rolls do not provide calibration and corrections for the BR component. The average BR component in the solar wind is expected to be small, because $BR \sim 1/R^2$, where R is the distance from the Sun. With $R \approx 100$ AU, $\langle BR \rangle \approx 0.0001$ nT, which is much smaller than the observed fields and also much smaller than the digitization level of the measurements. At this location the termination shock is not likely to change the field direction by a large amount. The assumption that $\langle BR \rangle = 0$ for 52 day intervals is probably valid in the inner heliosheath, although it need not be valid in the yet to be observed middle heliosheath.

[12] The widths of the two peaks are not constrained by the assumption that $\langle BR \rangle = 0$. The widths of the λ distributions with peaks near 90° and 270° are $w = 30° \pm 5°$ and $35° \pm 3°$, respectively. Thus the widths of the two peaks are the same within the uncertainties derived from the fits.

[13] The areas of the two peaks of the λ distribution in Figure 3a are $A_{d1} = 1630 \pm 240$ and $A_{d2} = 3800 \pm 250$ for the peak near 90° and near 270°, respectively. The larger peak for fields directed away from the Sun in the spiral direction is not expected, since V1 is at a latitude of 34°N, and the magnetic field in the Sun's northern hemisphere is predominantly toward the Sun.

[14] The distribution of daily averages of δ measured in the heliosheath from DOY 1–308, 2005 is shown in Figure 3b. A good fit to this distribution ($R^2 = 0.93$) is also obtained with a Gaussian function, $\delta = \delta_o + (A_d/(w \times \sqrt{(\pi/2)})) \times \exp(-2 \times ((\delta - \delta_c)/w)^2)$, with the parameters $\delta_o = 7° \pm 7°$, $\delta_c = 7° \pm 3°$, $w = 53° \pm 9°$, and $A_d = 4890 \pm 1070$. Again the uncertainties are only the statistical errors associated with the fit. The width of the δ distribution, $w = 53° \pm 9°$ appears to be

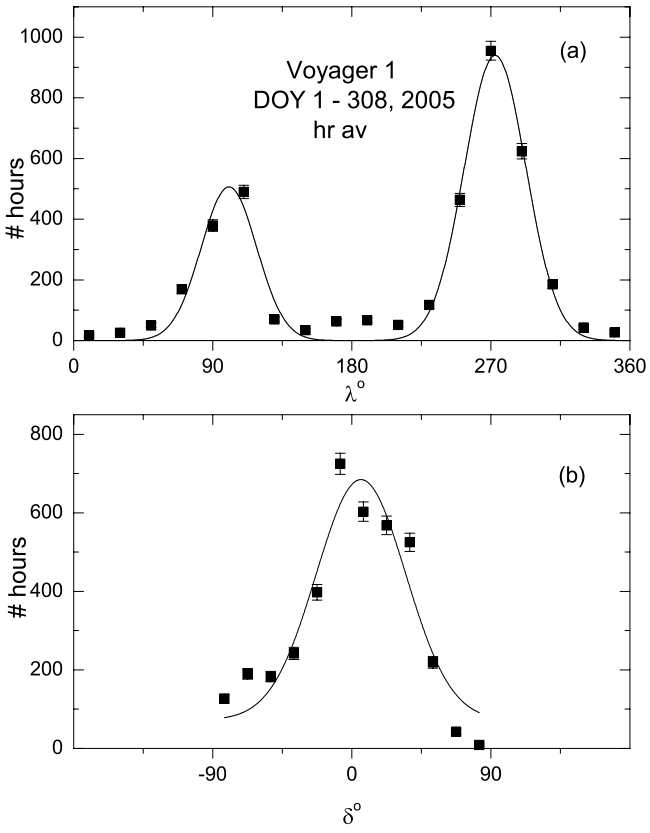

Figure 4. (a) Distribution of hourly averages of the azimuthal angle. (b) Distribution of hourly averages of the elevation angle.

somewhat larger than the widths of the λ distributions, but one cannot conclude that this is actually so given the uncertainties. The peak of the distribution of daily averages of δ is at $\delta \approx 0°$ within the uncertainties, consistent with the spiral angle and the definition of the R,T,N coordinate system used.

2.4. Distributions of Hour Averages of Magnetic Field Directions

[15] The distributions of hour averages of λ and δ, respectively are shown in Figure 4. The curves are fits to Gaussian distributions, as in Figure 3. The coefficient of determination $R^2 = 0.98$ indicates a good fit to the observed λ distribution. The peaks occur at $\lambda = 100° \pm 2°$ and $273° \pm 1°$, consistent with the spiral angle and the results obtained with the daily averages of λ. The widths of these two peaks are $w = 36° \pm 4°$ and $40° \pm 2°$, respectively. The areas of the peaks near 90° and 270° are $A_{h1} = 22800 \pm 2000$ and $A_{h2} = 47000 \pm 2200$, respectively, again indicating that the magnetic fields are directed primarily away from the Sun along the spiral direction. The ratio of the areas for the hour averages $A_{h1}/A_{h1} = 2.1 \pm 0.2$ is consistent with the ratio for the daily averages $A_{d2}/A_{d1} = 2.3 \pm 0.4$.

[16] The distribution of hour averages of the elevation angles δ is shown in Figure 4b. A Gaussian fit gives $R^2 = 0.93$. The peak is at $\delta = 6° \pm 3°$, close to zero, as one expects for a Parker spiral magnetic field. The width is $w = 58° \pm 10°$, similar to the width of the distribution of daily averages of δ ($53° \pm 9°$).

3. Multifractal Structure

3.1. Introduction

[17] The existence of a multifractal scaling symmetry in the large-scale fluctuations of the magnetic field strength $|\mathbf{B}|$ in the solar wind was first demonstrated by *Burlaga* [1991]. Multifractal scaling symmetry represents a hierarchical structure in phase space, in contrast to the uniformly occupied phase space of Boltzmann-Gibbs (B-G) statistical mechanics. Multifractal structure was observed in magnetic field data from Voyager 2 (V2) near 25 AU during 1987–1988 on scales from 16 hours to 21 days [*Burlaga*, 1991]. Multifractal structure of $|\mathbf{B}|$ was observed at 1 AU [*Burlaga*, 1992] and out to 85 AU during all phases of the solar cycle [e. g. *Burlaga*, 1995, 2004; *Burlaga et al.*, 2003a]. Some aspects of the multiscale statistical structure of the large-scale heliospheric magnetic field strength fluctuations has been predicted by a deterministic MHD model using input data from 1 AU [*Burlaga et al.*, 2003a].

[18] This section demonstrates the existence of multifractal structure in the large-scale magnetic fluctuations in the heliosheath. The observed structure can be described by the generalized multiplicative binomial model of *Meneveau and Sreenivasan* [1987]. The relation between the multifractal structure of $|\mathbf{B}|$ in the heliosheath and that in the distant supersonic solar wind is also discussed.

3.2. Evidence for Multifractal Structure in the Heliosheath

[19] Since the multifractal structure represents a scaling symmetry, and since it is convenient to work with powers of 2, we consider observations of $|\mathbf{B}|$ made by V1 in the heliosheath from DOY 1 through DOY 256 (2^8), 2005. The corresponding observations of $|\mathbf{B}|$ and estimates of the uncertainties (both random and systematic errors) are shown in Figure 1a. It is necessary to work with daily averages, because there are large data gaps each day. Thus we consider scales from $\tau = 2^0 = 1$ day to $2^7 = 128$ days.

[20] The theory of multifractals has been discussed by many authors [see, e.g., *Stanley and Meakin*, 1988; *Tel*, 1988]. This paper employs the methods used for identifying and describing multifractal structure in the heliospheric magnetic field introduced by *Burlaga* [1991] and reviewed by *Burlaga* [1995, chapter 9]. The magnetic flux is considered as a probability measure distributed on a continuous set (the time interval of the observations). The measure on the interval $[t_i, t_i + \tau_n]$ (where τ_n is the scale and i identifies the day number) is the ratio $Bn(t_i; \tau_n)$ of the average of the successive τ-day averages of $B(t_i)$ to the average of all the daily averages ($\tau = 0$) of $B(t_i)$, $\langle|\mathbf{B}(t_i)|\rangle$).

[21] Given the observed magnetic field strength normalized by its average value, $B(t_i) := |\mathbf{B}|/\langle|\mathbf{B}|\rangle$, one searches for multifractal structure by examining averages $\langle Bn^q\rangle$ of the qth moments of B(t) on various timescales $\tau_n = 2^n$, where n is an integer. If the magnetic field strength profile has a multifractal structure, then

$$\langle Bn^q\rangle \sim \tau_n^{s(q)} \quad (1)$$

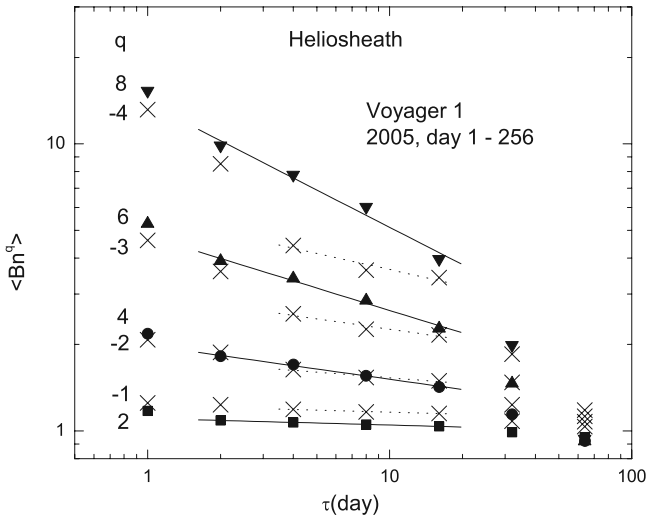

Figure 5. Averages of the qth moments of the successive τ-hour averages of B(t) versus scale τ.

over some range of scales. Here q is a real number; the positive and negative values of q single out peaks and troughs in B(t), respectively. From the observed B(t) we compute $\langle Bn^q \rangle$ as a function of scale τ for each of several integer values of q, $-10 < q < 1$ 0. Figure 5 shows the points $(\tau_n, \langle Bn^q \rangle)$ for $q = -1, -2, -3$, and -4 (denoted by "$\times$") and for $q = 2$, 4, 6 and 8 (solid symbols). The points $(\tau_n, \langle Bn^q \rangle)$ for each of the positive (negative) values of q fall on straight lines in the log-log plot in the range of scales from $\tau = 2$ to 16 days (4 to 16 days). The slopes of these lines, s(q) (points (q_i, s_i)) are plotted in Figure 6, together with the error bars. For a fractal (monofractal), s(q) would vary linearly with q. Figure 6 shows that the slopes vary nonlinearly with q in the range $-3 \leq q \leq 5$, demonstrating that multifractal structure exists in the magnetic field of the inner heliosheath.

3.3. Generalized Dimensions

[22] One way to describe multifractal structure is by the "generalized dimensions" $D_q(q)$, [see, e.g., *Hentschel and Procaccia*, 1983; *Sreenivasan*, 1991; *Beck and Schlögl*, 1993, and references in therein] which are related to s(q) by

$$D_q(q) = 1 + s(q)/(q - 1) \tag{2}$$

A plot of D_q versus q for the values of D_q from (2) for $-3 \leq q \leq 5$ is shown by the open circles in Figure 7. The error bars are very small for q near 1 and increase as the magnitude of q increases. There is no point for $q = 1$, because of the singularity in (2) at that value, which corresponds to the (constant) average value of $\langle Bn \rangle$. For $q = 0$, D_q is the capacity dimension, D_q (0) (approximately the Hausdorf dimension), which is equal to 1 within the uncertainties, as expected since the measure is distributed on a continuous line segment (the time interval under consideration). The curve in Figure 7 is a cubic fit to the observations, $D_q = (1.0000 \pm 0.0004) - (0.0115 \pm 0.0002)\, q - (1.01 \pm 0.66) \times 10^{-4}\, q^2 + (1.15 \pm 0.17) \times 10^{-4})\, q^3$, which provides a good fit to the data (coefficient of determination = 0.9997). The "intermittency exponent" of the fluctuations is given by

$$\mu = -2d/dq\left[D_q(q)\right]|_{q=0} \tag{3}$$

For fractal (self-affine) fluctuations, such as Brownian motion, $\mu = 0$. Differentiating the cubic fit, $D_q(q)$, we obtain $\mu = 0.023 \pm 0.002$. Thus the large-scale fluctuations of the magnetic field in the inner heliosheath are intermittent.

[23] *Meneveau and Sreenivasan* [1987] introduced a model (the "p model") to describe multifractal structure of the velocity in intermittent turbulence. This model was used by *Burlaga* [1991, 1992] to model the large-scale magnetic field strength fluctuations in the solar wind. The p model is a binomial multiplicative cascade model, constructed as follows: In our case, we start with a uniform distribution of magnetic flux on the interval [1, 256] with $\langle B(t) \rangle = 1$. Divide the time interval into two equal parts. Put a fraction p of the magnetic flux on one part chosen at random and a fraction $(1 - p)$ of the magnetic flux in the second part. This first iteration produces a signal that is a step function, a histogram with two bars. The randomly selected bar has a normalized magnetic field strength $p \times 2$, and the second bar has strength $(1 - p) \times 2$. The average normalized magnetic field in the signal (the two bars) is 1. In the second iteration, one repeats the process just described for each of the two bars, giving 4 bars and a value of B for each. Repeating this process 8 times gives 2^8 bars (256 1-day intervals) and a p-dependent value of B on each interval. One thereby creates a realization of the binomial process which is an approximation to the observed magnetic signal B(t) on some range of scales.

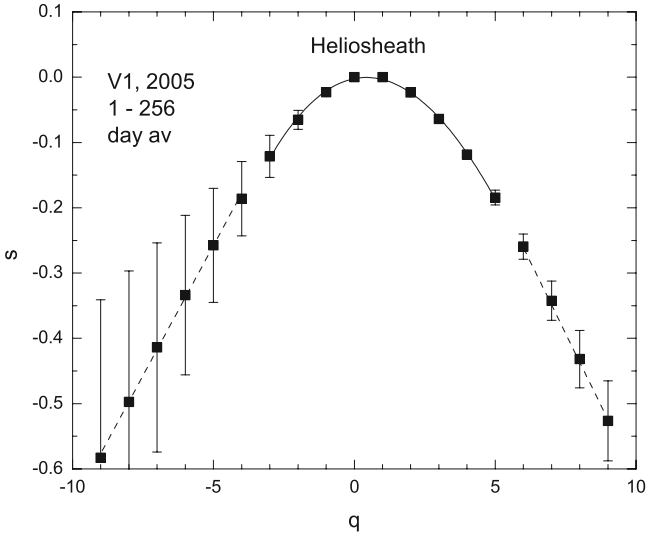

Figure 6. Slopes of the lines in Figure 5 versus q. Near $q = 0$ the slope s varies nonlinearly with moment q, indicating the existence of multifractal structure. The dashed lines showing a linear variation of s with q indicate that the data are not adequate to determine moments for $q \geq 6$ and $q \leq -4$.

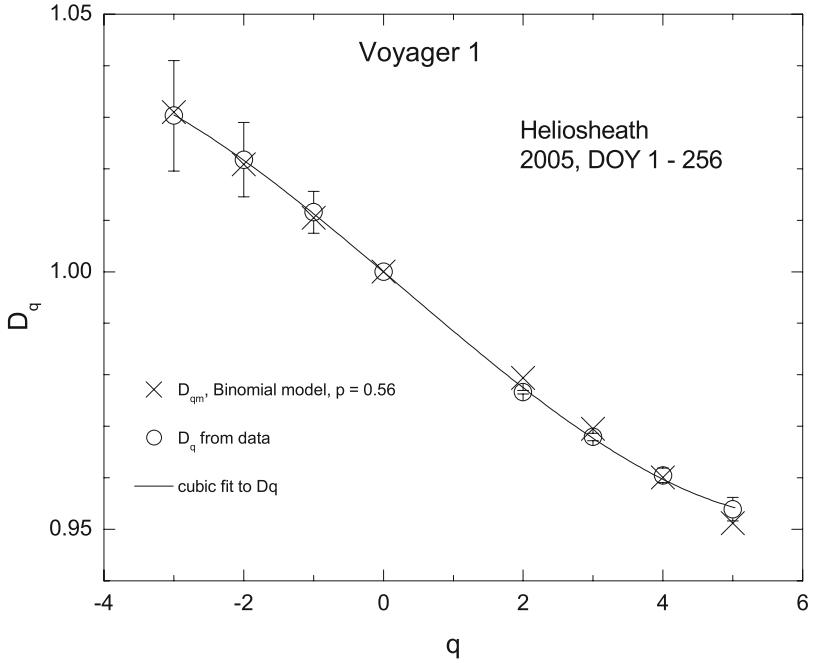

Figure 7. Generalized dimensions D_q versus q determined from the observations (open circles) and the p model with p = 0.56 (cross), together with a cubic fit to the data shown by the curve.

[24] The p model gives the generalized dimensions as a function of q and parameter p, namely [*Meneveau and Sreenivasan*, 1987],

$$D_q(q;p) = \log_2 [p^q + (1-p)^q]^{1/(1-q)} \quad (4)$$

Choosing p = 0.560 (putting 56% of the flux on one randomly chosen half of an interval and 44% on the other half), one obtains the crosses in Figure 7. The p model with p = 0.560 provides an excellent fit to the observations of $D_q(q)$ for $-3 \leq q \leq 5$. Although this range of q is very limited, it is a critical range that determines p accurately. The intermittency exponent for the p model is

$$\mu = \log_2 (4p(1-p))^{-1} \quad (5)$$

With p = 0.560 ± 0.001, equation (5) gives μ = 0.021 ± 0.001, in agreement with the intermittency exponent derived above from the observations using equation (3).

3.4. Multifractal Spectrum

[25] A second way to describe the multifractal structure is by the "multifractal spectrum" f(α) [*Halsey et al.*, 1986; *Sreenivasan*, 1991; *Stanley and Meakin*, 1988; *Tel*, 1988]

$$\alpha = d/dq\left[(q-1)D_q(q)\right] \quad (6)$$

$$f(\alpha) = q\,\alpha(q) - (q-1)D_q(q) \quad (7)$$

This gives the scaling exponent α of B on a subset of the interval having a fractal dimension f(α). The multifractal spectrum is more formal than the generalized dimensions $D_q(q)$, which describe the deviations from fractal behavior,

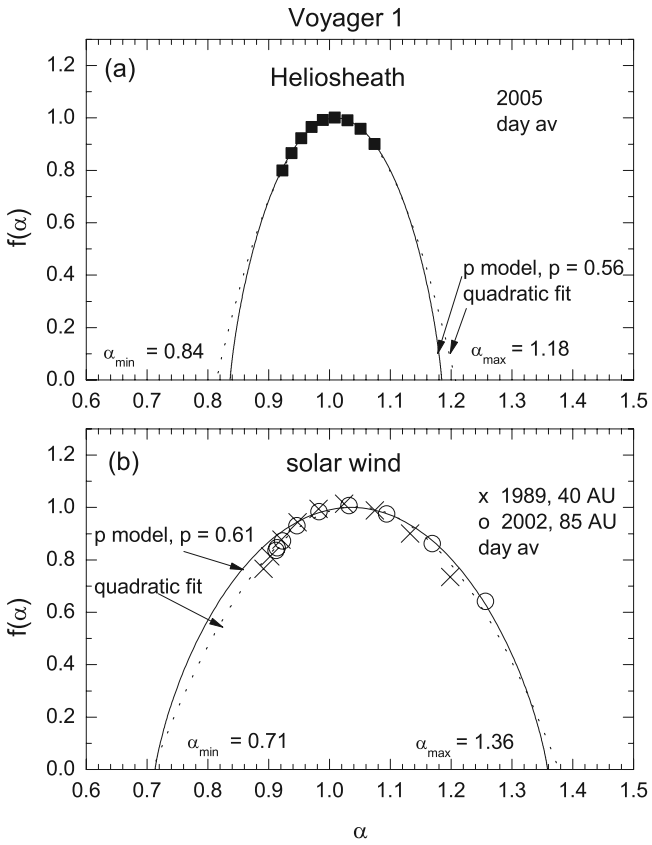

Figure 8. (a) Multifractal spectrum observed in the heliosheath (points) together with a quadratic fit (dashed curve) and a fit to the p model with p = 0.56 (solid curve). (b) Multifractal spectrum observed in the distant solar wind (points) together with a quadratic fit (dashed curve) and a fit to the p model with p = 0.61 (solid curve).

but its shape, position and width show graphically the nature of the multifractal structure. We shall comment on this below.

[26] Using the cubic fit to the observations of $D_q(q)$ given by the open circles in Figure 7, we obtain the corresponding points for $f(\alpha)$ shown by the solid squares in Figure 8a. Of particular interest are the values where $f(\alpha) = 0$, α_{min} and α_{max}. As discussed by *Meneveau and Sreenivasan* [1987], α_{min} is the generalized ("Rényi") dimension D_q in the limit $q \rightarrow \infty$ and α_{max} is the generalized dimension D_q in the limit $q \rightarrow -\infty$. $D(+\infty) = \alpha_{min}$ and $D(-\infty) = \alpha_{max}$ describe the scaling behavior on the set of time intervals where the measure is most concentrated (spikes in B) and least concentrated (minima in B), respectively. Unfortunately, the observations of $f(\alpha)$ are all above $\approx$0.8 for the heliosheath data, requiring a large extrapolation to obtain α_{min} and α_{max}. The limited range of observed values of $f(\alpha)$ is related to the limited range $-3 \leq q \leq 5$ for which we can determine D_q from the heliosheath observations. This in turn is related to the relatively small size of the data set. We extrapolate the available observations of $f(\alpha)$ to small and zero values of $f(\alpha)$ using models.

[27] One way to estimate α_{min} and α_{max}, used in previous studies [*Burlaga et al.*, 2003b; *Burlaga and Viñas*, 2005a], is to fit the observed values of (α_i, f_i) with a quadratic or cubic polynomial and extrapolate to $F = 0$. A quadratic fit, the dotted curve in Figure 8a, fits the observations very well, and gives $(\alpha_{min}, \alpha_{max}) = (0.82, 1.19)$, but one can question the extrapolation to $F = 0$. A cubic fit gives similar values, $(\alpha_{min}, \alpha_{max}) = (0.83, 1.24)$, but the extrapolation is again questionable. A second way to estimate α_{min} and α_{max} is to fit the data using a model such as the p model. With $p = 0.560 \pm 0.001$ derived above from the observations of D_q versus q in Figure 7, the p model gives $\alpha_{min} = D_{q \rightarrow \infty} = \log_2 p^{-1} = 0.84 \pm 0.01$ and $\alpha_{max} = D_{q \rightarrow -\infty} = \log_2 (1-p)^{-1} = 1.18 \pm 0.01$ for the heliosheath magnetic field observations. The multifractal spectrum derived from the p model with $p = 0.560$, the solid curve in Figure 8a, provides an excellent fit to the data ($R^2 = 0.99973$), and it is close to the quadratic fit.

3.5. Relation Between Multifractal Spectra in the Heliosheath and Solar Wind

[28] Multifractal spectra of magnetic field strength fluctuations observed by V1 in the solar wind are shown in Figure 8b. The crosses and circles in Figure 8b show observations made in 1989 between 36.3 to 38.8 AU [*Burlaga et al.*, 2003b] and in 2002 between 83.4 to 86.9 AU [*Burlaga*, 2004], respectively. The multifractal spectrum observed at $\approx$40 AU by V1 in 1989 was predicted by *Burlaga et al.* [2003b] using a deterministic MHD model with observations at 1 AU as input.

[29] The daily averages of $|\mathbf{B}|$ observed in the supersonic solar wind by V1 during 1989 and 2002 have a multifractal structure in the range of scales from $\tau \approx 2$ to 32 days and 2 to 16 days, respectively. For 1989 and 2002, quadratic fits to the observed points in the multifractal spectrum give $(\alpha_{min}, \alpha_{max}) = (0.70 \pm 0.06, 1.4 \pm 0.1)$ and $(0.76 \pm 0.06, 1.4 \pm 0.1)$, respectively [*Burlaga and Viñas*, 2005b]. Thus the observations of α_{min} and α_{max} for the 1989 data are essentially the same as those for the 2002 data, within the uncertainties. The points for both 1989 and 2002 scatter about a single curve that gives $f = 0$ at $\alpha_{min} = 0.71 \pm 0.06$ and $\alpha_{max} = 1.4 \pm 0.1$. This result is consistent with a quasi-stationary metastable state of the solar wind between 40 and 85 AU organized about a multifractal attractor in phase space, as noted by *Burlaga and Viñas* [2005b].

[30] The p model with $p = 0.610$ (solid curve in Figure 8b) gives a good fit to the distant solar wind observations for all but the smallest values of α. The quadratic model and the p model with $p = 0.610 \pm 0.001$ give the same values of α_{min} and α_{max} within the uncertainties. The p model gives $\alpha_{min} = D_{q \rightarrow \infty} = \log_2 p^{-1} = 0.71 \pm 0.02$ and $\alpha_{max} = D_{q \rightarrow -\infty} = \log_2 (1-p)^{-1} = 1.36 \pm 0.04$ for the magnetic field in the distant solar wind, consistent with the solar wind observations discussed in the previous paragraph.

[31] The multifractal spectrum of the magnetic field fluctuations in the heliosheath (Figure 8a) is narrower than that in the distant solar wind (Figure 8b). In particular $(\alpha_{min}, \alpha_{max}) = (0.84 \pm 0.01, 1.18 \pm 0.01)$ in the heliosheath and $(0.71 \pm 0.02, 1.36 \pm 0.04)$ in the distant solar wind. The widths of the multifractal spectra are related to the values of p in the p model, namely, $p = 0.56$ and 0.61 for the heliosheath and solar wind, respectively. These values of p for the magnetic field strength may be compared with the value $p = 0.7$ for the p model of small-scale intermittent speed fluctuations in the solar wind [*Burlaga*, 1991] and laboratory [*Anselmet et al.*, 1984]. The value $p = 0.7$ gives a relatively broad multifractal spectrum, with $(\alpha_{min}, \alpha_{max}) = (0.51, 1.74)$. As p decreases, the multifractal spectrum $f(\alpha)$ becomes narrower. In the limit $p \rightarrow 0.5$ (equal magnetic flux on each of the two subintervals, hence no redistribution of magnetic flux) the width approaches 0, $(\alpha_{min}, \alpha_{max}) \rightarrow (1, 1)$.

[32] The capacity dimension D(0) is the value of F for the α at which $df/d\alpha = 0$, corresponding to f_{max}. For the heliosheath, $f_{max} = 1.004$ at $\alpha = 1.01$; for the solar wind $f_{max} = 1.003$ at $\alpha = 1.004$. Thus the capacity dimension ("box" dimension) $D(0) = 1$, within the measurement uncertainties, for both the heliosheath and the solar wind; this is expected since the measure is distributed on a line in the measured time series. Similarly the information dimension D(1) is the value of F for the α at which $df/d\alpha = 1$ [*Beck and Schlögl*, 1993]. For the heliosheath and solar wind, $D_{HS}(1) = 0.99$ and $D_{SW}(1) = 0.98$, respectively, again consistent with 1.

[33] The intermittency exponent of the large-scale fluctuations in the normalized magnetic field strength B(t) decreases by a factor of 3.4 from $\mu = 0.072$ in the distant solar wind to $\mu = 0.021$ in the heliosheath. (The intermittency exponent for speed fluctuations in the distant solar wind is smaller by a factor of 3.5 than the value $\mu \approx 0.25$ for turbulence observed at small scales in the laboratory [*Anselmet et al.*, 1984]). The decrease in intermittency of the large-scale fluctuations in B (and the width of the multifractal spectrum) from the distant solar wind to the heliosheath might be caused by the passage of the solar wind fluctuations through the termination shock and/or relaxation in the heliosheath. There is no model of these processes at present. One might speculate that the high thermal speed and pressure in the heliosheath allows large unbalanced gradients in B to smooth out more rapidly than in the solar wind, thereby reducing the peaks in B that cause relatively high intermittency in the solar wind. The fluctua-

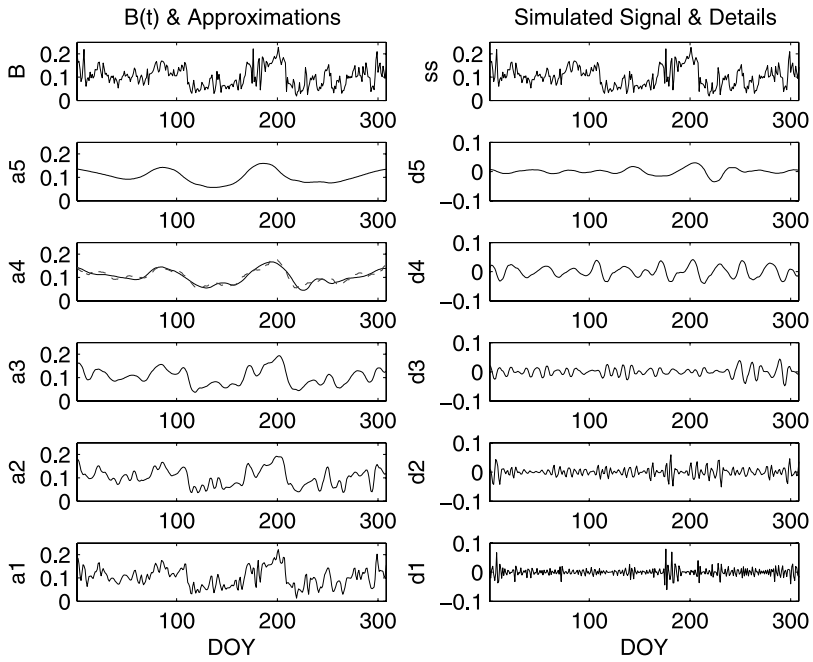

Figure 9. Wavelet analysis of the observed magnetic field strength profile (B, top left). The "approximations" are shown with increasing detail for a5 to a1, respectively. The "details" for successively smaller scales are shown for d5 to d1, respectively. The signal constructed from the approximations and details is shown for ss (top right).

tions in the heliosheath are closer to thermal equilibrium than those in the solar wind. Nevertheless, multifractal (nonthermal) structure is still present in the inner heliosheath on scales from 2 to 16 days.

4. Wavelet Decomposition

[34] Another way to analyze the multiscale structure of B(t) in the heliosheath is by means of wavelets [*Strang and Nguyen*, 1996]. The basic idea is to decompose the signal in a hierarchal way (e.g., powers of 2), using functions called wavelets. There are many kinds of wavelets, and the choice among them is subjective. We choose the Daubechies wavelets (dbn) because they are standard and simple, give smooth profiles, and they give approximations close to the running averages at the larger scales. More complicated wavelets such as symlets and the discrete approximation of Meyer wavelets give very similar results. In particular, we choose the wavelet db5 (decomposition to level 5) after examining several other levels, because this revealed the essential features without an excessive number of panels in the plot. The resulting decomposition of the daily averages of B(t) measured from DOY 1 to 308, 2005 is shown in Figure 9. The observations shown in Figure 9 (top left) are the same as those in Figure 1a.

[35] The wavelet decomposition of the signal is given by the "approximations" (a1, a2, a3, a4 and a5) and by the "details" (d1, d2, d3, d4, and d5). The approximations and details are related by the equation $a(i-1) = ai + di$, $i = 1 \ldots 5$. For example, the approximation a4 is equal to a5 + d5, where a5 is a large-scale approximation to B(t) and detail d5 is a correction that provides smaller-scale features, giving the signal a4.

[36] Running 16 day averages of the observed B(t) are shown by the dashed curve in the panel for a4 in Figure 9. Clearly, a4 is approximately the same as the 16-day running average of B(t). The signal a4 captures the basic features of the observations that one "sees" on a scale of 308 days. Choosing a higher level decomposition, db7, would show one cycle of a sine wave for a6 and a trend line for a7, which we do not consider.

[37] Since $a(i-1) = ai + di$, $i = 1 \ldots 5$, a simulated signal "ss" can be reconstructed from the formula ss = a0 = a1 + d1 = a5 + (d5 + d4 + d3 + d2 + d1). The resulting ss is shown in Figure 9 (top right). Despite the low level of the decomposition, the simulated signal is remarkably similar to the observed signal B versus DOY in Figure 9 (top left). By comparing a5 with a4, a4 with a3, etc., one can see how the signal is built up by adding further details di at each scale.

[38] Taking a5 as the basic structure of the signal B(t), the multiscale structure on smaller scales is described by d1, d2, d3, d4, and d5 in Figure 9. The relatively high-resolution details d1 and d2 show a bursty, intermittent, spiky structure that is familiar in solar wind turbulence, which gives large non-Gaussian tails in the distribution of dBn at the smallest scales [*Burlaga et al.*, 2006b]. The intermittency is also present in d3, but less markedly so, with a relatively small amplitude compared to the other di. A transition to a different kind of structure is observed between d3 and d4. This transition corresponds to the transition from Tsallis distributions with extended tails to Gaussian distributions, as discussed by *Burlaga et al.* [2006b].

[39] Note that d4 is a quasi-sinusoidal signal. Fourier analysis shows a strong peak at 28.4 ± 1.5 days, close to the solar rotation period of 26 days (Figure 10). This contribution to the approximations first appears in a3, where it is evident that the contribution is a significant part of the

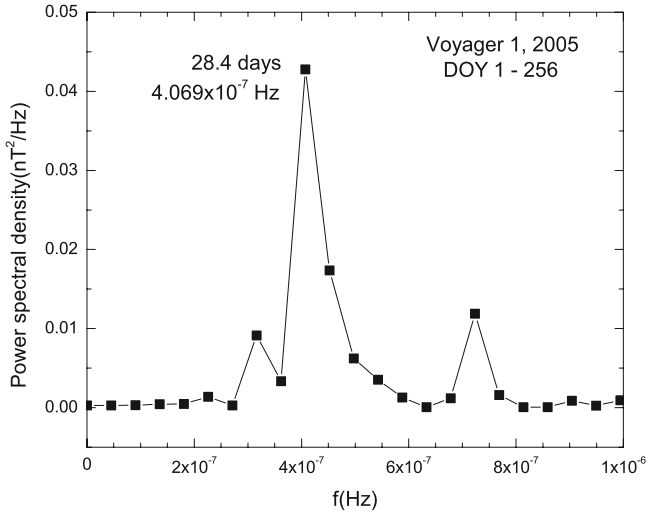

Figure 10. Power spectral density of the detail signal d4 versus DOY in Figure 10. There is a strong peak at ≈28.4 days, close to the solar rotation period, suggesting that effects of the solar rotation can be seen in the heliosheath.

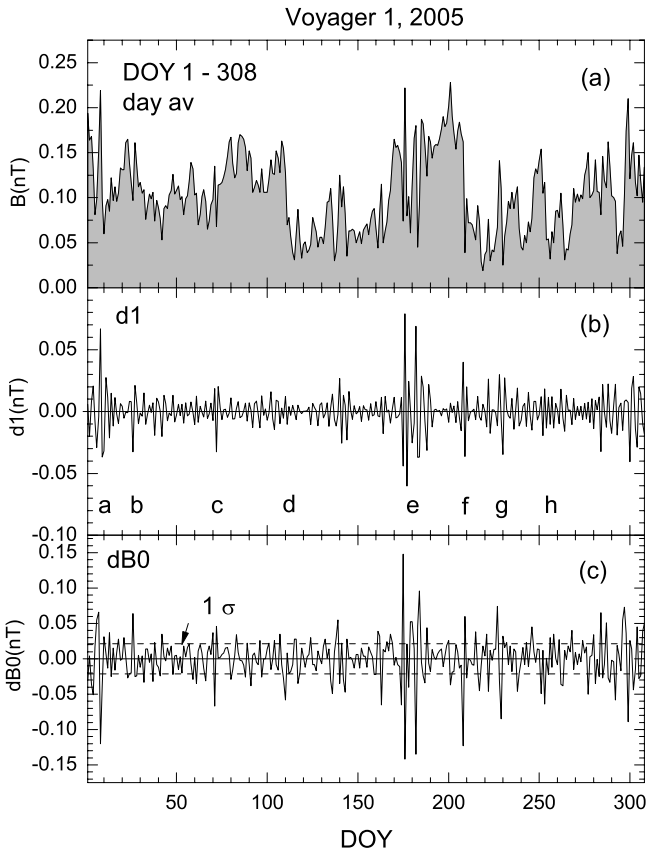

Figure 11. (a) Observations of daily averages of the magnetic field strength B as a function of time for DOY 1–308. (b) Detail signal d1 from Figure 10. Extrema indicate the presence of large changes in B(t). (c) Change in the magnetic field strength from one day to the next (dB0) as a function of time. Extrema of dB0 indicate the presence of "jumps" in the signal B(t).

signal. We suggest that the effects of solar rotation were being observed in the heliosheath at ≥95 AU.

[40] Finally, note that the intense bursts and spikes in d1 identify notable regions in the observed signal B(t). In fact, d1(t) is very similar to dB0(t) = B(ti + 1 day) − B(ti), as shown in Figure 11. Both the details d1 from wavelet analysis and the running differences dB1 of successive daily averages of B identify the large, abrupt changes in B(t). Some of the largest peaks or "bursts" in abs(d1) and abs(dB0) are labeled a through h in Figure 11; these are discussed in section 5.

5. Large Changes in |B|

[41] As discussed above and by *Burlaga et al.* [2006b], there are a number of large changes in B on a scale of 1–4 days in the interval from DOY 1–308, which contribute to the multifractal structure of B(t) and non-Gaussian tails of the Tsallis distributions of dBn. The aim of this section is to show that there is no single type of fluctuation in B that causes the large changes in B. We find several types of structures related to large peaks in |d1| and |dB0|. These peaks, which exceed the 1 σ uncertainties in dB0, are labeled a, b, c.... in Figure 11b.

[42] The large "spike" in |dB0| labeled "a" in Figure 11b is related to a large narrow enhancement in B that was discussed by *Burlaga et al.* [2006a], who noted that it corresponds to a change in the energetic particle profile. The cause of the enhancement is not known, but high-resolution observations show that it is associated with a series of large-amplitude wavelike pulsations. A smaller increase in |dB0|, marked "b" in Figure 11b, is related to a

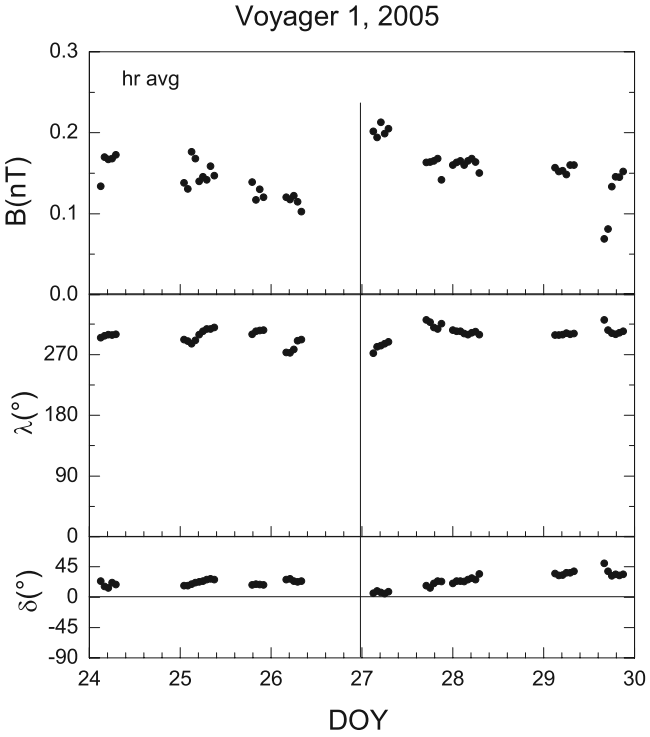

Figure 12. Hour averages of **B** showing that the jump in B(t) on DOY 26 which is primarily a step-like change in the magnetic field strength B.

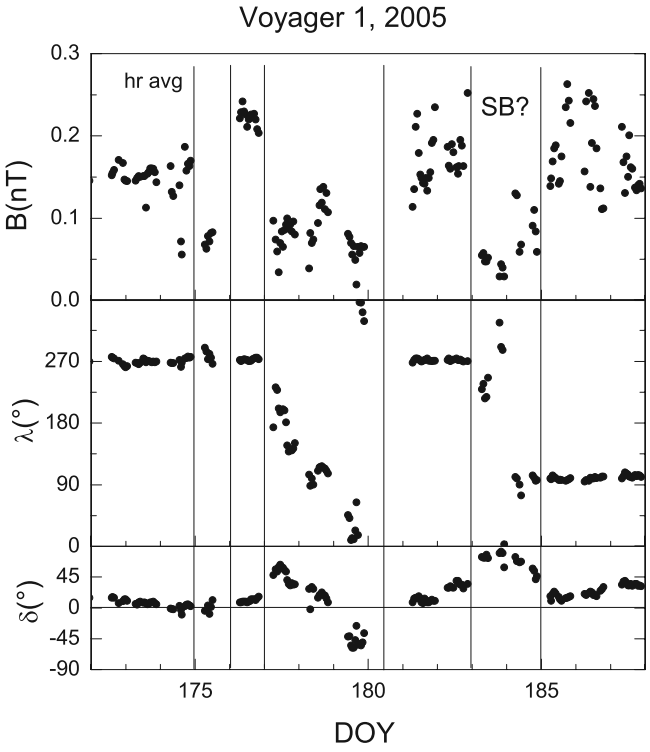

Figure 13. Hour averages of **B** showing a series of large jumps in B in B(t), some of which are associated with changes in direction.

"jump" in B (Figure 12), which is not accompanied by a significant change in magnetic field direction. The jump resembles a tangential "discontinuity" or perhaps a shock. We cannot determine its width because the jump occurs in a data gap, and we cannot determine whether it is a pressure balanced structure or a shock owing to the absence of plasma data on V1. We must wait until V2 enters the heliosheath to better understand such jumps. A relatively small extremum in |dB0|, marked "d" in Figure 11b, is associated with what appears to be associated with the boundary of a filament (see Figure 11a). This feature, which was discussed by *Burlaga et al.* [2006a], was associated with a sector boundary. Clearly it is associated with the entry of V1 into a flow with different polarity and presumably different density and/or temperature.

[43] A series of peaks in |dB0|, marked by "e" in Figure 11b, is associated with large fluctuations and spikes in B (Figure 11a). A close-up of this region, based on hour averages of **B** from DOY 172 to 188, is shown in Figure 13. There are large fluctuations in both the magnitude of B and its direction in this interval. There are two large jumps in B without changes in the direction on ≈DOY 175.0 and 176.0. A large decrease in B on ≈DOY 177.0 marks a transition to a region in which the magnetic field direction is changing appreciably in 3 days. Another large jump in B occurs in a data gap on ≈DOY 180, across which there is a large change in the direction of **B**. Finally, on DOY 183 there appears to be a crossing of something resembling a sector boundary, in which λ rotates from 270° to 90°, δ rotates northward through a large angle and back, and the magnetic field is very weak. There is a large scatter of B from DOY 180 to 188, which is related to small-scale structures that will be discussed in another paper.

[44] A large decrease in B, which appears to be the boundary of a large filament, was observed on DOY 209, 2005 (see Figure 11a and the peak in |dB0|marked "f" in Figure 11b. This feature is shown more clearly in the hour averages of **B** (Figure 14). The decrease in B occurs at a sector boundary, across which λ increases from ≈90° to ≈270°. Again, one sees low values of B and large values of δ at the sector boundary, which moved past the spacecraft for at least 12 hours. This sector boundary resembles those studied by *Burlaga et al.* [2003b] and that in Figure 13. In the supersonic solar wind it is not unusual to find weak fields and large elevation angles in a sector boundary, but it is unusual to find a large change in B across a sector boundary [see, e.g., *Burlaga et al.*, 2003b]. Another spike in B in Figure 11a, associated with the peak marked "g" in Figure 11b, was observed on DOY 227–230. Hour averages of **B** presented in Figure 15 show that **B** was relatively strong and uniform in direction within the spike. The fields were weak, and thus the angles were poorly determined before and after the spike.

[45] Finally, we consider the structure associated with the large jump and relatively broad spike in B seen in Figure 11a on ≈DOY 250 and in the peak in |dB0| labeled "h" in Figure 11b. This feature is shown in more detail by the hour averages of **B** in Figure 16. The "spike" in B was a region of strong fields from DOY 248 through 254. In this period the direction of **B** was very uniform, but there

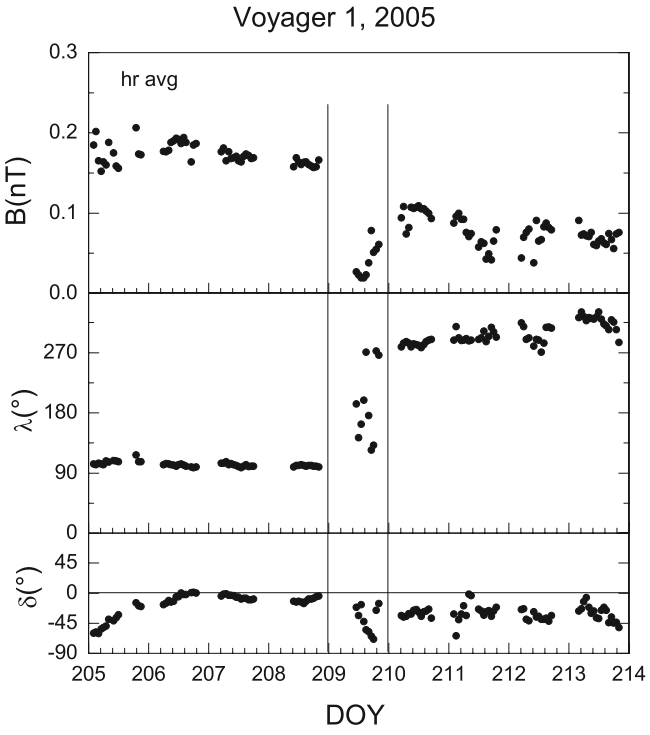

Figure 14. Hour averages of **B** showing two jumps in B related to a depression in the magnetic field strength at a sector boundary.

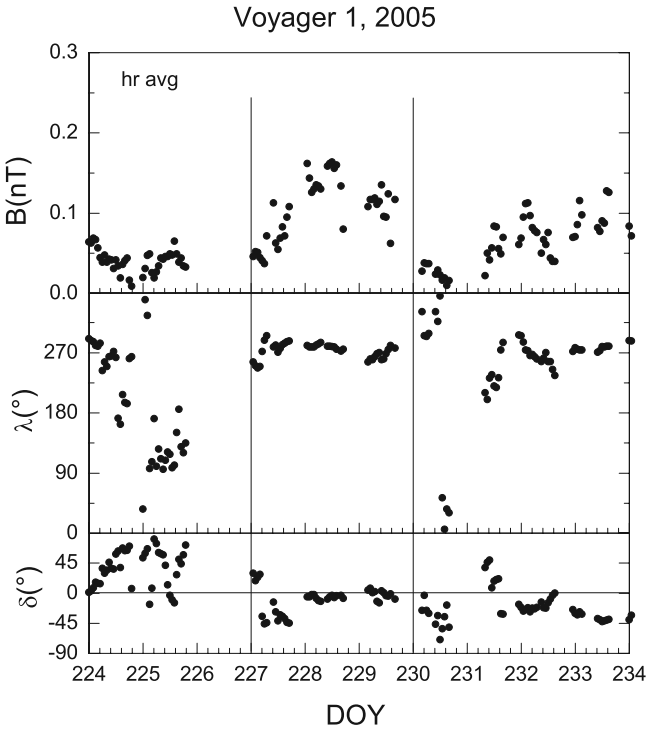

Figure 15. Hour averages of **B** showing two jumps in B bounding a region with relatively strong magnetic fields.

were large fluctuations in B. The fluctuations in B are the result of small-scale structures that are not resolved by the hour averages; the structures will be discussed in a separate paper. Figure 16 shows that the broad spike in B was followed by a sector boundary that moved past V1 from ≈DOY 255 to ≈260. Within this sector boundary, B was relatively weak on average (but with large fluctuations), and δ rotated from zero to large values and back to zero. Across the sector boundary λ changed from a sector with $\lambda \approx 270°$ to a sector with $\lambda \approx 90°$.

6. Summary and Discussion

[46] We analyzed the structure of the magnetic field in the heliosheath observed by Voyager 1 (V1) from DOY 1 to 308, 2005. The average magnetic field strength in this interval is $\langle B \rangle = 0.104 \pm 0.002$ nT, where the uncertainty here is the standard error in the mean. The standard deviation is SD = 0.043 nT, and the minimum and maximum values of B are 0.02 nT and 0.23 nT, respectively. The profile of B(t) shows large jumps in B and gives the appearance of an underlying filamentary or multiple "flux tube-like" structure. Daily averages of the azimuthal angle λ and elevation angle δ suggest that a sector structure seems to be present in λ. Some features which can be identified as sectors and sector boundaries were observed.

[47] The daily and hourly averages of B in the inner heliosheath have Gaussian distributions, in contrast to the nearly lognormal distributions found in the solar wind. It is significant that the B(t) observations have a Gaussian distribution even though the profile seems to be filamentary with some large jumps and peaks in B. The 2 σ widths of the daily and hourly distributions of B are (0.048 ± 0.008) nT and (0.059 ± 0.008) nT, respectively, suggesting a scale invariance of the distribution of B on scales from 1 hour to 1 day.

[48] The distributions of daily and hourly averages of the azimuthal angles λ each show two Gaussian peaks; 104° ± 2° and = 270° ± 1° for the daily averages and at 100° ± 2° and 273° ± 1° for the hourly averages. These values are close to the Parker spiral values for large distances from the Sun, 90° and 270°. The 2σ widths of the λ distributions with peaks near 90° and 270° are respectively 30° ± 5° and 35° ± 3°, for the daily averages and 36° ± 4° and 40° ± 2° for the hourly averages. Thus the widths of the two peaks are the same within the uncertainties, although the peaks for

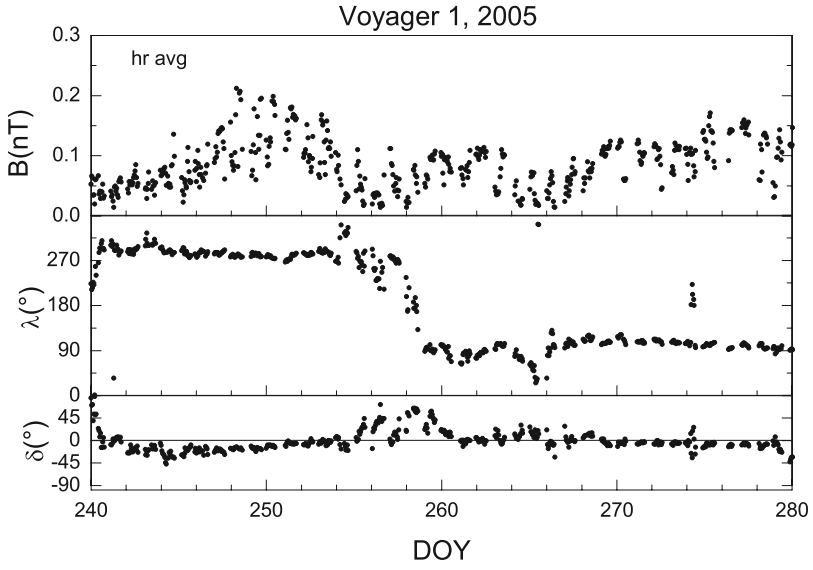

Figure 16. Hour averages of **B** showing jumps in B ahead of a sector boundary during an interval in which there were large fluctuations in B at small scales.

the hourly data appear to be somewhat broader. The ratio of the areas of the two peaks of the λ distribution near 270° to that near 90° is 2.3 ± 0.4 for the daily averages. The larger peak for fields directed away from the Sun in the spiral direction is not expected, since V1 is at a latitude of 34° in the northern solar hemisphere, and the magnetic field of the Sun in its northern hemisphere is predominantly toward the Sun at this phase of the solar cycle.

[49] The daily and hourly averages of δ measured in the heliosheath have Gaussian distributions whose widths are $2\sigma = 53° \pm 9°$ and $58° \pm 10°$, respectively. The peaks of the distributions are at $\delta \approx 0°$ and $6° \pm 3°$ for the daily and hourly values, consistent with the spiral angle.

[50] Since both the distribution of azimuthal and elevation angles in the inner heliosheath are consistent with the Parker spiral for the supersonic solar wind, we conclude that the Termination Shock did not produce a significant change in the distribution of the magnetic field directions as it entered the inner heliosheath along the trajectory of V1. This is consistent with the termination shock as a quasi-perpendicular shock at this location.

[51] We found that the magnetic field strength in the inner heliosheath has a multifractal structure on scales from ≈2 to 16 days. The multifractal structure represents a scaling symmetry. One way to describe multifractal structure is by the ''generalized dimensions'' $D_q(q)$. The observations of D_q versus q for $-3 \leq q \leq 5$ can be described by the cubic polynomial. The ''intermittency exponent'' of the fluctuations is given by $\mu = -d/dq[D_q(q)]|_{q=0}$ from which we obtain $\mu = 0.021 \pm 0.001$. Thus the large-scale fluctuations of the magnetic field in the inner heliosheath are intermittent. The binomial multiplicative cascade model (the ''p model'') with p = 0.560 provides an excellent fit to the observations of $D_q(q)$ for $-3 \leq q \leq 5$. The intermittency exponent computed from the p model with $p = 0.560 \pm 0.001$ is $\mu = 0.021 \pm 0.001$.

[52] A second way to describe multifractal structure is by the ''multifractal spectrum'' $f(\alpha)$. This gives the scaling exponent α of B on a subset of the interval having a fractal dimension $f(\alpha)$. The values where $f(\alpha) = 0$, α_{min} and α_{max}, describe the scaling behavior on the set of time intervals where the measure is most concentrated (spikes in B) and least concentrated (minima in B), respectively. Both a quadratic polynomial and the p model fit the observed values of (α_i, f_i) very well. Extrapolating the fits to $f = 0$ gives $(\alpha_{min}, \alpha_{max}) = (0.82, 1.19)$ for the quadratic fit and $(\alpha_{min}, \alpha_{max}) = (0.84 \pm 0.01, 1.18 \pm 0.01)$ for the p model.

[53] The multifractal spectrum observed by V1 in the solar wind in 1989 is essentially the same as that for the 2002 solar wind data, consistent with a quasi-stationary metastable state of the solar wind between ≈40 and ≈85 AU organized about a multifractal attractor in phase space. The p model with $p = 0.610 \pm 0.001$ gives a good fit to the multifractal spectrum of B in the distant solar wind. We found that $(\alpha_{min}, \alpha_{max}) = (0.84 \pm 0.01, 1.18 \pm 0.01)$ in the heliosheath and $(\alpha_{min}, \alpha_{max}) = (0.71 \pm 0.02, 1.36 \pm 0.04)$ in the distant solar wind. Thus the multifractal spectrum of the magnetic field fluctuations in the heliosheath is narrower than that for the magnetic field fluctuations in the distant solar wind. The intermittency exponent of the large-scale fluctuations in the normalized magnetic field strength B(t) decreases by a factor of 3.4 from $\mu = 0.072$ in the distant solar wind to $\mu = 0.021$ in the heliosheath. There is no model of the specifics of these processes at present. The fluctuations in the heliosheath are closer to statistical equilibrium than those in the solar wind. Nevertheless, multifractal (nonequilibrium) structure is still present in the inner heliosheath at scales from ≈2 to 16 days.

[54] We also analyzed the multiscale structure of B(t) in the heliosheath by the method of wavelets. We choose the wavelet db5 and a decomposition to level 5. Taking a5 as the basic structure of the signal B(t), the multiscale structure on smaller scales is described by d1, d2, d3, d4, and d5. The relatively high-resolution details d1 and d2 show a bursty, intermittent, spiky structure that gives large non-Gaussian tails in the distribution of dBn at the smallest scales. The intermittency is also present in d3, but less markedly so, with a relatively small amplitude compared to the other di. A transition to a different kind of structure is observed between d3 and d4, corresponding to a transition from Tsallis distributions with long tails to Gaussian distribution functions.

[55] The approximation a4 is approximately the same as the 16-day running average of B(t). It captures the basic ''intermediate-scale'' features of the observations. The d4 is a quasi-sinusoidal signal with a dominant period of 28 days, suggesting that the effects of solar rotation are being observed in the heliosheath at 95 AU.

[56] There are a number of large changes in B on a scale of 1–8 days in the interval from DOY 1–256, which contribute to the multifractal structure of B(t) and non-Gaussian tails of the Tsallis distributions of dBn. No single type of fluctuation in B causes the large changes in B. Such structures include (1) a large narrow peak in B; (2) a step-like jump in B with no significant change in direction, possibly related to a tangential ''discontinuity'' or a shock; (3) the boundary of a filament that was associated with a sector boundary; (4) large fluctuations related to multiple jumps in **B**; (5) a broad sector boundary in which B drops to relatively low values; and (6) a ''spike'' in B with strong fields observed for ≈6 days in which there were large fluctuations in B as a result of small-scale structures that are not resolved by the hour averages.

[57] **Acknowledgments.** The data in this paper are from the magnetic field experiment on Voyager 1. N. F. Ness was partially supported by grant NNG04GB71G to the Catholic University of America. T. McClanahan and S. Kramer carried out the processing of the data. The ''0 tables'' were computed by Roberto Borda.

[58] Wolfgang Baumjohann thanks Manfred Leubner and another reviewer for their assistance in evaluating this paper.

References

Anselmet, F., Y. Gagne, E. J. Hopfinger, and R. A. Antonia (1984), High-order velocity structure functions in turbulent shear flows, *J. Fluid Mech.*, *140*, 63.

Arimitsu, T., and N. Arimitsu (2000), Tsallis statistics and fully developed turbulence, *J. Phys. A*, *33*, L235.

Arimitsu, T., and N. Arimitsu (2002), Tsallis statistics and turbulence, *Chaos Solitons Fractals*, *13*(3), 479.

Axford, W. I. (1972), The interaction of the solar wind with the interstellar medium, in *Solar Wind*, edited by C. P. Sonett, P. J. Coleman, and J. M. Wilcox, *NASA Spec. Publ.*, *308*, 609.

Beck, C., and F. Schlögl (1993), *Thermodynamics of Chaotic Systems*, chapter 11, Cambridge Univ. Press, New York.

Behannon, K. W., M. H. Acuna, L. F. Burlaga, R. P. Lepping, N. F. Ness, and F. M. Neubauer (1977), Magnetic-Field experiment for Voyager-1 and Voyager-2, *Space Sci. Rev.*, *21*, 235.

Burlaga, L. F. (1991), Multifractal structure of the interplanetary magnetic field: Voyager 2 observations near 25 AU, 1987–1988, *Geophys. Res. Lett.*, *18*, 69.

Burlaga, L. F. (1992), Multifractal structure of the magnetic field and plasma in recurrent streams at 1 AU, *J. Geophys. Res.*, *97*(A4), 4283.

Burlaga, L. F. (1995), *Interplanetary Magnetohydrodynamics*, Oxford Univ. Press, New York.

Burlaga, L. F. (2001), Lognormal and multifractal distributions of the heliospheric magnetic field, *J. Geophys. Res.*, *106*(A8), 15,917.

Burlaga, L. F. (2004), Multifractal structure of the large-scale heliospheric magnetic field strength fluctuations near 85 AU, *Nonlinear Processes Geophys.*, *11*(4), 441.

Burlaga, L. F., and A. F. Viñas (2005a), Tsallis distributions of the large-scale magnetic field strength fluctuations in the solar wind from 7 to 87 AU, *J. Geophys. Res.*, *110*, A07110, doi:10.1029/2005JA011132.

Burlaga, L., and A. Viñas (2005b), Triangle for the entropic index q of non-extensive statistical mechanics observed by Voyager 1 in the distant heliosphere, *Physica A*, *356*, 375.

Burlaga, L. F., C. Wang, and N. F. Ness (2003a), A model and observations of the multifractal spectrum of the heliospheric magnetic field strength fluctuations near 40 AU, *Geophys. Res. Lett.*, *30*(10), 1543, doi:10.1029/2003GL016903.

Burlaga, L. F., N. F. Ness, and J. D. Richardson (2003b), Sectors in the distant heliosphere: Voyager 1 and 2 observations from 1999 through 2002 between 57 and 83 AU, *J. Geophys. Res.*, *108*(A10), 8028, doi:10.1029/2003JA009870.

Burlaga, L. F., N. F. Ness, M. H. Acuña, R. P. Lepping, J. E. P. Connerney, E. C. Stone, and F. B. McDonald (2005), Crossing the termination shock into the heliosheath: Magnetic fields, *Science*, *23*, 2027.

Burlaga, L., N. Ness, and I. H. Acuña (2006a), Magnetic fields in the heliosheath: Voyager 1 observations, *Astrophys. J.*, *642*, 584–592.

Burlaga, L., A. Viñas, N. Ness, and I. H. Acũna (2006b), Tsallis statistics of the magnetic field in the heliosheath, *Astrophys. J.*, *644*, L83–L86.

Decker, R. B., S. M. Krimigis, E. C. Roelof, M. E. Hill, T. P. Armstrong, G. Gloeckler, D. C. Hamilton, and L. J. Lanzerotti (2005), Voyager 1 in the foreshock, termination shock, and heliosheath, *Science*, *23*, 2020.

Gurnett, D. A., and W. S. Kurth (2005), Electron plasma oscillations upstream of the solar wind termination shock, *Science*, *23*, 2025.

Halsey, T. C., M. H. Jensen, L. P. Kadanoff, I. Procaccia, and B. I. Shraiman (1986), Fractal measures and their singularities: The characterization of strange sets, *Phys. Rev. A*, *33*(2), 1141.

Hentschel, H. G. E., and I. Procaccia (1983), The infinite number of generalized dimensions of fractals and strange attractors, *Physica D*, *8*(3), 435.

Hundhausen, A. J. (1972), *Coronal Expansion and Solar Wind*, Springer, New York.

Leubner, M. P., and Z. Vörös (2005), A nonextensive entropy approach to solar wind intermittency, *Astrophys. J.*, *618*, 547.

Meneveau, C., and K. R. Sreenivasan (1987), Simple multifractal cascade model for fully-developed turbulence, *Phys. Rev. Lett.*, *59*(13), 1424.

Parker, E. N. (1963), *Interplanetary Dynamical Processes*, Wiley-Interscience, Hoboken, N. J.

Sreenivasan, K. R. (1991), Fractals and multifractals in fluid turbulence, *Annu. Rev. Fluid Mech.*, *23*, 539.

Stanley, H. E., and P. Meakin (1988), Multifractal phenomena in physics and chemistry, *Nature*, *335*, 405.

Stone, E. C., A. C. Cummings, F. B. McDonald, B. C. Heikkila, N. Lal, and W. R. Webber (2005), Voyager 1 explores the termination shock region and the heliosheath beyond September 2005, *Science*, *23*, 2017.

Strang, G., and T. Nguyen (1996), *Wavelets and Filter Banks*, Wellesley-Cambridge Press, Wellesley, Mass.

Tel, T. (1988), Fractals, multifractals, and thermodynamics, *Z. Naturforsch A*, *43*, 1154.

M. H. Acũna, Planetary Magnetospheres Laboratory, Code 695, NASA Goddard Space Flight Center, Greenbelt, MD 20771, USA.

L. F. Burlaga, Laboratory for Solar and Space Physics, Code 612.2, NASA Goddard Space Flight Center, Greenbelt, MD 20771, USA. (leonard.f.burlaga@nasa.gov)

N. F. Ness, Institute for Astrophysics and Computational Sciences, Catholic University of America, Washington, DC 20064, USA.